

# Universal ultrabright source of entangled photon states: generation and tomographic analysis of Werner states and of Maximally Entangled Mixed States

G. Di Nepi, F. De Martini, M. Barbieri and P. Mataloni

*Dipartimento di Fisica and Istituto Nazionale per la Fisica della Materia*

*Università di Roma "La Sapienza", Roma, 00185 - Italy*

## Abstract

A novel ultrabright parametric source of polarization entangled photon pairs with striking spatial characteristics is reported. The distribution of the output electromagnetic  $\mathbf{k}$ -modes excited by Spontaneous Parametric Down Conversion and coupled to the output detectors can be very broad. It could coincide with the *full set* of phase-matched excited modes, at least *in principle*. In this case a relevant *conditional quasi-pure* output state should be realized. By these (approximate) states realized over a full *Entanglement-Ring* output distribution, the non local properties of the generated entanglement has been tested by standard Bell measurements and by Ou-Mandel interferometry. A novel "*mode-patchwork*" technique based on the quantum superposition principle is adopted to synthesize in a straightforward and reliable way any kind of *mixed-states*, of large conceptual and technological interest in modern Quantum Information. Tunable Werner states and Maximally Entangled Mixed States (MEMS) have indeed been created by the new technique and investigated by quantum tomography. A thorough study of the entropic and nonlocal properties of these states has been undertaken experimentally and theoretically, by a unifying variational approach. PACS: 03.67.Mn, 03.65.Ta, 03.65.Ud, 03.65.Wj.

## I. INTRODUCTION

Entanglement, "the characteristic trait of quantum mechanics" according to Erwin Schroedinger, is playing an increasing role in nowadays physics [1]. It is the irrevocable signature of quantum nonlocality, i.e. the scientific paradigm today recognized as the fundamental cornerstone of our yet uncertain understanding of the Universe. The striking key process, the "bolt from the blue" [i.e. from the skies of Copenhagen] according to Leo Rosenfeld [2], was of course the EPR discovery in 1935 followed by a much debated endeavour ended, in the last few decades by the lucky emergence of the Bell's inequalities and by their crucial experimental verification [3]. In the last years the violation of these inequalities has been tested so many times by optical experiments that (almost) no one today challenges the completeness of quantum nonlocality.

In the modern science of quantum information (QI) entanglement represents the basis of the exponential parallelism of future quantum computers [4], of quantum teleportation [5,6] and of some kinds of cryptographic communications [7].

It appears largely significant that the most successful and reliable applications of entanglement have been obtained so far in the field of quantum optics. There the electromagnetic modes are associated with "qubits" which are generally encoded by the field polarization ( $\pi$ ) [8]. This type of qubit encoding is precisely the one considered in the present work. The  $\pi$ -entanglement arises within the spontaneous emission process (Spontaneous Parametric Down Conversion: SPDC) in a nonlinear optical crystal under suitable conditions, as we shall see shortly. In this process, a pair of correlated photons are generated at wavelengths (wl)  $\lambda_1$  and  $\lambda_2$  and momenta  $\hbar\mathbf{k}_1$  and  $\hbar\mathbf{k}_2$  by a quantum electrodynamical (QED) annihilation of a pump photon with wl  $\lambda_p$  and momentum  $\mathbf{k}_p$ . Conservation of energy,  $\lambda_1^{-1} + \lambda_2^{-1} = \lambda_p^{-1}$  and of the momentum, i.e. *phase-matching* condition  $\mathbf{k}_1 + \mathbf{k}_2 = \mathbf{k}_p$  leads to frequency and  $k$ -vector correlation of the emitted photons. In condition of entanglement the bipartite Hilbert space  $H_1 \otimes H_2$  with  $\dim(H_1) = \dim(H_2) = 2$  is spanned by the four Bell-state entangled basis,

$$|\Psi_{\pm}\rangle = 2^{-\frac{1}{2}} (|H_1, V_2\rangle \pm |V_1, H_2\rangle), |\Phi_{\pm}\rangle = 2^{-\frac{1}{2}} (|H_1, H_2\rangle \pm |V_1, V_2\rangle) \quad (1)$$

where  $H$  and  $V$  correspond to the horizontal and vertical linear field's polarizations and the shorthand:  $|X_1, Y_2\rangle \equiv |X\rangle_1 \otimes |Y\rangle_2$  and will be used henceforth. The source of entanglement adopted today almost exclusively in quantum optics is based on SPDC in a Type II non-collinear "phase matched" nonlinear (NL) crystal in which a pair of mutually orthogonally polarized photons is generated over a set of correlated directions corresponding to two different emission cones [9]. The cones intersect each other in two particular correlated modes with k-vectors  $\mathbf{k}_i$ ,  $i = 1, 2$ . The overall quantum state emitted over these two modes may be expressed by either Bell state  $|\Psi_{\pm}\rangle$ , depending on a preset NL crystal orientation. By a careful spatial selection of the two correlated k-vectors  $\mathbf{k}_i$ , e.g. by two narrow pinholes, a high purity entangled state may be generated by this kind of source. The typical achievable coincidence count rate is of the order of few hundreds  $\text{sec}^{-1}$  in a typical case involving a  $1\text{mm}$  thick NL crystal excited by a  $100\text{mW}$  UV pump laser. More recently, Paul Kwiat has realized a different source of  $\pi$ -entangled pairs, an order of magnitude brighter than the previous one, based on SPDC emission by a set of two thin, orthogonally oriented Type I crystal slabs placed stuck in mutual contact [10].

In the present work we report on a novel SPDC source of polarization-entangled pairs, recently developed in our laboratory [11], that we believe represents the ultimate solution in the framework of quantum optics in terms of universality and flexibility of generation of entangled states. The new solution, besides realizing the maximum attainable "quantum efficiency" ( $QE$ ), i.e. relative "brightness", allows the detection of *all* SPDC entangled pairs emitted by SPDC over the *entire* set of wavevectors excited by any parametric scattering process. In particular, we have investigated in the present work the most efficient,  $\lambda$ -degenerate process:  $\lambda_1 = \lambda_2 = 2\lambda_p$ . Note briefly in this connection that the present source, when applied to any Bell inequality test, allows to overcome substantially the *quantum-efficiency* "loophole", which refers to the lack of *detection* of *all couples* of emitted correlated photons [12]. This loophole should indeed be considered to be properly ascribable to the limited

efficiency of the detectors as well as to the loss of the pairs created in any single QED spontaneous emission process that do not reach the detectors for geometrical reasons. We shall account about this subtle process in a forthcoming paper dealing with nonlocality tests undertaken by means of inequalities (Bell-Bohm) [3,13] with and without making recourse to inequalities (Hardy) [14].

The present work is mostly devoted to investigate theoretically and experimentally a quite new branch of QI, the one concerned with the properties of several relevant families of *mixed-entangled states*. Because of the unavoidable effects of the decohering interactions indeed these states are today considered the basic constituents of modern QI and Quantum Computation as they limit the performance of all quantum communication protocols including quantum dense coding [15] and quantum teleportation [5,6]. It is not surprising that in the last few years, within an endeavour aimed at the use of *mixed-states* as a practical resource, an entire new branch of arduous mathematics and topology has been created to investigate the unexplored theory of the *positive-maps* (*P-maps*) in Hilbert spaces in view of the assessment of the “*residual entanglement*” and of the establishment of more general “*state-separability*” criteria [16–18]. Very recently this ambitious study has reached results that are conceptually relevant, as for instance the discovery of a *discontinuity* in the structure of the *mixed-state* entanglement. Precisely, the identification of two classes: the *free-entanglement*, useful for quantum communication, and the *bound-entanglement*, a *non-distillable* mysterious process, elicited a fascinating new horizon implied by the basic question: what is the role of *bound* entanglement in Nature [19]?

A consistent and wide range investigation of these useful and outmost appealing aspects of modern physics requires the availability of a universal, flexible source by which entangled *pure* as well *mixed-states* of *any* structure could be easily engineered in a reliable and reproducible way. The novel high-brilliance source described in the present work indeed possesses these properties and, consistently with the above considerations, it will be applied first to the realization and to a quantum tomographic analysis of the Werner states with variable mixing parameters [20–22]. At last, the relevant “*maximally entangled mixed states*”

(MEMS), today of large conceptual and technological interest, have been easily created and tested by the same techniques [23].

The work is organized as follows: in Section II the high-brightness source is fully described. Moreover the high quality of the realized output entangled state is demonstrated by a Bell-inequality test showing the attainment of a nonlocal interferometric visibility as large as  $V \geq 0.94$  and a violation of a Bell inequality by 213 standard deviations. Section III reports on a novel "patchwork" method to generate a full set of Werner states. In addition, the results of a quantum tomographic investigation of their properties shall be reported. In Section IV the methods of the previous Section will be extended to a theoretical and experimental study of the MEMS. In Section V the EPR nonlocality of the MEMS and of the Werner states shall be taken up in a unifying manner by a variational analysis of the correlation functions. Finally, the foreseeable perspectives of the new method will be outlined in Section VI.

## II. THE HIGH BRIGHTNESS SOURCE OF ENTANGLEMENT

The active element of the new source of polarization-entangled photon pairs consisted of a single Type-I NL thin crystal slab,  $\beta$ -barium-borate (BBO), excited in two opposite directions ( $\mathbf{k}_p, -\mathbf{k}_p$ ) by a UV pump beam with wl  $\lambda_p$ , back-reflected by a spherical mirror ( $M$ ): Figure 1. Each of the two equal but independent SPDC processes generated pairs of correlated photons with wavelengths (wl)  $\lambda_i$ , ( $i = 1, 2$ ), *equal* polarizations ( $\pi$ ) and with a spatial distribution of the corresponding, mutually correlated k-vectors  $\mathbf{k}_i$  consisting of two equal, opposite *circular* cones (dubbed as "k-cones") with axes  $\mathbf{k}_p, -\mathbf{k}_p$  [9,10]. While all the relevant features of the present source are shared by all *non-degenerate* phase-matched wl configurations, i.e.  $\lambda_1^{-1} + \lambda_2^{-1} = \lambda_p^{-1}$  with  $\lambda_1 \neq \lambda_2$ , our present demonstration has been (and the present discussion will be) carried out mostly for the *degenerate* case for simplicity and without loss of generality:  $\lambda_1 = \lambda_2 = \lambda = \lambda_p/2 = 727.6nm$ . Suppose that the NL crystal orientation is preset as to generate SPDC pairs on both k-cones with any linear polarization,

say  $\pi = H$ . Each pair of each  $\mathbf{k}$ -cone is then emitted with a product state  $|H_1, H_2\rangle$  over its own 4-dimensional Hilbert space. Suppose now that the two  $\mathbf{k}$ -cones are made to overlap into a *single* one with axis  $\mathbf{k}_p$ , i.e. directed towards the right hand side (r.h.s.) of Fig.1, by back-reflection over  $M$  of the  $\mathbf{k}$ -cone with axis  $-\mathbf{k}_p$ . If in the flight from the crystal to  $M$  and back the polarization of the corresponding emitted pairs is flipped by any unitary transformation, i.e.  $H_i \rightarrow V_i$  and a phase  $\phi$  is added, the state of the pair detected on the (r.h.s.) of Fig.1 is the *entangled* state:

$$|\Phi\rangle = 2^{-\frac{1}{2}} (|H_1, H_2\rangle + e^{i\phi}|V_1, V_2\rangle) \quad (2)$$

Since this argument holds for *any* pair of correlated  $\mathbf{k}_i$ -vectors emitted with equal probability and equal wl  $\lambda$ , all diametrically opposite points of the spatial circle obtained by interception with a plane of the output cone, i.e. belonging to the "*entanglement-ring*" as we shall see shortly, are correlated by the same entanglement condition and then represented by  $|\Phi\rangle$ . Of course, as for all quantum interference phenomena, the  $\mathbf{k}$ -cone overlapping should be perfect as to realize the "*in principle indistinguishability*" of the actual origin of the detected pair for any set of *ideal* detectors coupled to the output of the source. All this represents the key process underlying the present work.

Let us now give more details of the apparatus (Fig. 1). A Type I, .5mm thick, crystal was excited by a slightly focused  $V$ -polarized cw  $Ar^+$  laser beam ( $\lambda_p = 363.8nm$ ) with wavevector  $-\mathbf{k}_p$ , i.e. directed towards the l.h.s. in Fig.1. The two photons had common  $H$  polarization and were emitted with *equal probability* over a corresponding pair of wavevectors belonging to the surface of a cone with axis  $-\mathbf{k}_p$  and aperture  $\alpha \simeq 2.9^\circ$ . The emitted radiation and the laser beam were then back-reflected by a spherical mirror  $M$  with curvature radius  $R = 15cm$ , highly reflecting both  $\lambda$  and  $\lambda_p$ , placed at a distance  $d = R$  from the crystal. A zero-order  $\lambda/4$  waveplate (wp) placed between  $M$  and the NL crystal, i.e. indicated as "*d-zone*" in Fig.1, intercepted twice both back-reflected  $\lambda$  and  $\lambda_p$  beams and then rotated by  $\pi/2$  the polarization of the back-reflected field with wl  $\lambda$  while leaving virtually undisturbed the polarization state of the UV pump beam. In facts, it was verified that the  $\lambda/4$  wp

acted closely as a  $\lambda_p/2$  wp since  $\lambda_p = 2\lambda$ . The phase  $\phi$  ( $0 \leq \phi \leq \pi$ ) of the generated pure entangled state, Eq.(2) was reliably controlled by micrometric displacements  $\Delta d$  of  $M$  along  $\mathbf{k}_p$ . The phase stability, representing the most challenging experimental problem, was solved by adoption of various tricks, among which vital was the use of the *same* back-mirror  $M$  for both wl's  $\lambda, \lambda_p$  (see Appendix A). A positive lens ( $f = 15cm$ ) transformed the overall emission *conical* distribution into a *cylindrical* one with axis  $\mathbf{k}_p$ , whose transverse circular section identified the “*Entanglement-ring*” (*E-ring*) with diameter  $D = 2\alpha F$ . Each couple of points symmetrically opposed through the center of the ring are then correlated by quantum entanglement, as said. An annular mask with diameter  $D = 1.5cm$  and width  $\delta = .07cm$  provided in the present experiment a very accurate spatial selection of the *E-ring*. This one was divided in two equal portions along a vertical axis by a prism-like two-mirror system and then focused by two lenses on the active surfaces of two independent photodiodes  $A$  and  $B$  (*Alice* and *Bob*) by which standard Bell measurements could be performed by means of polarization analyzers ( $\vec{\pi}$ ). The detectors were silicon-avalanche mod. SPCM-AQR14 with quantum efficiency  $QE = 65\%$  and dark count rate  $\simeq 50s^{-1}$ . Typically, two equal interference filters, placed in front of the  $A$  and  $B$  detectors, with bandwidth  $\Delta\lambda = 6nm$ , determined the *coherence-time* of the emitted photons:  $\tau_{coh} \approx 140fsec$ . Optionally, the focusing could have been done on the ends of two optical fibers that could convey the radiation to two far apart detection stations  $A$  and  $B$ .

The insertion of one (or several) waveplates of filters partially (or fully) intercepting the radiation associated with the  $\mathbf{k}$ -cones in (or outside) the  $d$ -zone allowed the realization of various configurations of relevant physical significance. For instance, the insertion of a zero-order  $\lambda/2$  wp in one of the output detection arms allowed to locally transform Eq.(2) into the state:

$$|\Psi\rangle = 2^{-\frac{1}{2}} (|H_1, V_2\rangle + e^{i\phi}|V_1, H_2\rangle) \quad (3)$$

Then, by easily setting  $\phi = 0$  or  $\phi = \pi$  Eq.1 could be locally transformed in any one of the remaining three Bell states. Furthermore and most important, the insertion of a zero-order

$\lambda_p/4$  wp in the  $d$ -zone and intercepting *only* the UV beam allowed the engineering of tunable *non maximally entangled* states. As shown by Lucien Hardy, by this class of states expressed as:

$$|\Phi\rangle = \alpha|H_1, H_2\rangle + \beta|V_1, V_2\rangle; \quad \alpha \neq \beta; \quad |\alpha|^2 + |\beta|^2 = 1 \quad (4)$$

the nonlocality of quantum mechanics could be tested without recourse to inequalities ("Hardy's ladder proof") [14]. In our system, the rotation of the UV wp by an angle  $\theta_p$  determines a  $\pi$ -rotation of the back-reflected UV pump beam respect to the optical axes of the (fixed) NL crystal slab. The consequent  $\theta_p$ -tunable unbalancement of the SPDC efficiencies over the two  $\mathbf{k}$ -cones affects the two interfering product-state terms in Eq.(2) by a coefficient  $\propto \cos^2 2\theta_p$ . By adjusting  $\theta_p$  in the range  $0 - \pi/4$ , the *degree of entanglement*  $\gamma = |\alpha/\beta|$  can be continuously tuned between 1 and 0. Successful, preliminary results of the Hardy's ladder proof obtained by adoption of the present source have been reported in [11]. More complete data will be reported elsewhere.

All these consideration are but a preliminary demonstration of the extreme flexibility of the present source. In the following Sections we shall learn how, by a simple "*patchwork*" technique approximately "*pure*" states can be easily transformed into "*mixed*" states with various degree of mixedness. This allowed us to undertake a comprehensive study of relevant quantum states as the Werner states and the Maximally Entangled Mixed States (MEMS).

### A. Generation of approximate conditionally pure-states

The structural characteristics of the quantum state of any photon pair generated by our source should be analyzed by accounting first for the excited electromagnetic (e.m.) modes which, in our case are grouped in correlated pairs by the 3-wave SPDC interaction. Assume that each SPDC  $\mathbf{k}$ -cone is represented by a linear superposition of  $N \gg 1$  correlated pairs of e.m. mode sets,  $\mathbf{k}_{ij} \equiv \{\mathbf{k}_{1j}, \mathbf{k}_{2j}\}$  where each component is a *plane-wave* mode represented by a  $k$ -vector  $\mathbf{k}_j$ . The symbol  $j$ , ranging from 1 to  $N$  represents the *full set* of e.m. modes that



are coupled to any elementary QED 3–wave parametric scattering process taking place in the NL crystal and whose excitation is dynamically allowed by the *phase-matching* conditions. The symbol  $i = 1, 2$  accounts, as previously, for the spin- $\frac{1}{2}$  Hilbert space finally coupled to the detectors  $A$  or  $B$ , respectively. Since only *one pair* of photons is detected at the output of the source, each of these  $\mathbf{k}_{ij}$  mode sets corresponds to a Fock 2–mode product-state that can be either  $|0, 0\rangle_j$  or  $|1_H, 1_H\rangle_j$  or  $|1_V, 1_V\rangle_j$ . These two last product-states correspond to the states expressed in a less precise form in Eq.(2). Finally, owing to the linearity of quantum mechanics, the overall *entangled-state* expressing a single pair emission and detected at the output of our source after  $\mathbf{k}$ -cone overlapping and  $\phi$ –phase delay may finally be expressed by the quantum superposition:

$$|\Phi\rangle = 2^{-\frac{1}{2}} \sum_{j:1}^N (|1_H, 1_H\rangle_j + e^{i\phi}|1_V, 1_V\rangle_j) \quad (5)$$

over a set of plane-wave modes, assumed here *discrete* for simplicity. This should be indeed the *exact* form of the output state of the source, if the *full set* of  $j$ -modes could be coupled to the cathode of the detectors  $A$  and  $B$ . Indeed, it is not difficult to find that this full coupling scheme is virtually *made possible* by the actual structure of our source in all possible wavelength configurations, either *degenerate* ( $\lambda_1 = \lambda_2$ ) or *non-degenerate* ( $\lambda_1 \neq \lambda_2$ ). In other words, an experiment may be conceived in principle (an approximate one is in fact in progress in our laboratory) by which the *full set* of QED excited modes at any wavelength, ranging from very large  $\lambda_i$  down to  $\lambda_i = \lambda_p$  can be coupled to the detectors *without* any geometrical constraint or spatial or  $\lambda$ -filtering. Of course, in this case severe limitations for a *full particle detection* come from the limited  $\lambda$ –extension of the photocathode *QE's* and of the performance of the optical components (mirrors, lenses etc.). Nevertheless, this does not affect *in principle* the *structural character* of the output entangled-state.

Note that in all SPDC-based quantum optics experiment carried out so far, the set of  $\mathbf{k}_{ij}$  modes coupled to the detectors was drastically reduced by the use of narrow spatial-filtering pinholes [6,8–10]. Actually, the goal there was the realization of particle detection over a *single* pair of correlated  $\mathbf{k}$ –vectors, i.e. only one  $j$  term of the distribution appearing in Eq.(5).

As a consequence, in all experiments performed thus far the drastically truncated sum in Eq.5 implied necessarily a *highly mixed* character of the output state. These considerations lead to at least two important consequences:

A) The *high-brilliance* of the source, due to the full output mode coupling was found experimentally to  $\simeq 2$  order of magnitudes larger than the conventional one based on SPDC excited by a UV laser with the same intensity.

B) The *quasi-purity* of the generated output state may be considered as follows. The well known *unitary* character of the quantum operator  $\hat{S}$  accounting for SPDC assures that the purity of the *input state* implies also the purity of the *output state*:  $|\Phi\rangle_{out} = \hat{S}|\Phi\rangle_{in}$  [24]. Adopting the common hypothesis of a undepleted "classical" pump beam, the input *pure state* is expressed by the overall vacuum-state character of the input modes of the 3-wave parametric interaction. Within the single-pair emission approximation, the output (pure) state  $|\Phi\rangle_{out}$  consists of the sum of the state  $|\Phi\rangle$ , given by Eq.(5), and of the vacuum-state expressing the *non realization* of the QED parametric scattering process in the NL crystal. As a consequence,  $|\Phi\rangle$  expressed by Eq.(5) *is not*, strictu sensu, a pure state but one out of a two components *mixture*. However, in the actual case of a *conditional experiment*, i.e. where the overall detection system is activated by a trigger pulse elicited by the source itself, the output vacuum-state contribution can be eliminated. In this case the output state  $|\Phi\rangle$  given by Eq. (2) may be considered a *pure* one. This last condition is usually referred to as expressing the "*conditional purity*" of the output state.

## B. Bell inequalities test

The  $|\Phi_{-}\rangle$  Bell state expressed by Eq.2 with  $\phi = \pi$ , i.e. a "singlet" has been adopted to test the violation of a Bell inequality by the standard coincidence technique and by the experimental configuration shown in Figure 1 [25]. According to the previous considerations, the distribution of active e.m. modes appearing in Eq. (5) and corresponding to the whole *E-ring* was spatially-filtered by the annular mask, as said. In spite of this drastically limiting

cutoff we refer to the output state as a *quasi-pure* state.

The adopted angle orientations of the  $\vec{\pi}$ -analyzers located at the  $A$  (1) and  $B$  (2) sites were:  $\{\theta_1 = 0, \theta'_1 = 45^\circ\}$  and  $\{\theta_2 = 22.5^\circ, \theta'_2 = 67.5^\circ\}$ , together with the respective orthogonal angles:  $\{\theta_1^\perp, \theta'^\perp_1\}$  and  $\{\theta_2^\perp, \theta'^\perp_2\}$ . By these values, the standard Bell-inequality parameter could be evaluated [26]:

$$S = |P(\theta_1, \theta_2) - P(\theta_1, \theta'_2) + P(\theta'_1, \theta_2) + P(\theta'_1, \theta'_2)| \quad (6)$$

where

$$P(\theta_1, \theta_2) = \frac{[C(\theta_1, \theta_2) + C(\theta_1^\perp, \theta_2^\perp) - C(\theta_1, \theta_2^\perp) - C(\theta_1^\perp, \theta_2)]}{[C(\theta_1, \theta_2) + C(\theta_1^\perp, \theta_2^\perp) + C(\theta_1, \theta_2^\perp) + C(\theta_1^\perp, \theta_2)]}$$

and  $C(\theta_1, \theta_2)$  is the coincidence rate measured at sites  $A$  and  $B$ . The measured value  $S = 2.5564 \pm .0026$  [11], obtained by integrating the data over 180s, corresponds to a violation as large as 213 standard deviations respect to the limit value  $S = 2$  implied by local realistic theories [3,26,27]. As for the full set of measurements reported in the present paper, the good performance was, of course partially attributable to the high brightness of the source by which a large set of statistical data could be accumulated in very short measurement times and with a low UV pump power.

The experimental data given in Figure 2 show the  $\vec{\pi}$ -correlation obtained by varying the angle  $\theta_1$  in the range  $(45^\circ - 135^\circ)$ , having kept fixed the angle  $\theta_2 = 45^\circ$ . The interference pattern shows the high degree of  $\pi$ -entanglement of the source. The measured visibility of the coincidence rate,  $V \geq 94\%$ , gives a further strong indication of the entangled nature of the state over the entire cone emission  $\mathbf{k}$ -cone, while the single count rates don't show any periodical fringe behaviour as expected. In the same Fig.2 the dotted line corresponds to the limit boundary between the quantum and the classical regimes [26] while the theoretical continuous curve expresses the *ideal* interferometric pattern with maximum visibility:  $V = 1$ .

The entanglement character of the source has been investigated by a standard Ou-Mandel interferometric test [11,28], in this case with the Bell state expressed by Eq.(3): Fig.3, inset. For this experiment the radius of the iris diaphragms ( $ID$ ) (Fig. 1) was set at  $r = 0.75mm$ .

The experimental results, shown in Fig. 3 and corresponding to the values  $\phi = \pi$  and  $\phi = 0$ , give a value of interference visibility:  $V \simeq 88\%$ . The FWHM ( $\simeq 35\mu m$ ) of the interference pattern is in good agreement with the expected value evaluated for a filter bandwidth  $\Delta\lambda = 6nm$ . In the same Fig. 3 the experimental results corresponding to the non-interference case  $\phi = \pi/2$  are also shown for comparison.

We have characterized the robustness and the brightness of the source by measuring coincidences for different values of radius  $r$  of the  $(ID)$ . This corresponds to select different portions of the  $E$ -ring, with area  $\mathcal{S} = 2D\delta \arcsin(\frac{r}{D})$  (Fig. 1, inset). The experimental results of Fig. 4 demonstrate that a coincidence rate larger than  $4 \times 10^3 \text{sec}^{-1}$  at a pump power  $P \simeq 100mW$  is measured over the entire  $E$ -ring with a still relevant value of visibility. This outperforms the overall collection efficiency of the SPDC process. By taking into account the UV pump power and the overall efficiency of the apparatus (transmission of the optical plates + detector  $QE's$ ), we can evaluate that the entangled photon pairs are generated at a rate larger than  $2 \cdot 10^5 s^{-1}$ . On the other hand, because of the continuous wave excitation regime, the NL parametric gain is so small,  $g < 10^{-3}$  that the ratio of the probabilities of simultaneous SPDC generation of 2 photon pairs and of a single pair is  $\leq 10^{-6}$ . As a consequence, the emission of a double pair is negligible with cw pumping.

The present demonstration has been carried out in the  $\lambda$ -degenerate condition, i.e. implying the largest QED emission probability according to NL Optics. Note however, as said, that the apparatus works, without any structural change for a very general  $\lambda$ -non-degenerate dynamics. This would allow, at least in principle and by the use of sufficiently broadband detectors, the simultaneous detection of the (almost) complete *set* of SPDC generated pairs.

Note the high structural flexibility of this novel SPDC source. Its structure indeed suggests the actual implementation of several relevant schemes of quantum information and communication, including entanglement multiplexing, joint entanglement over  $\vec{\pi}$  and  $k$ -vector degrees of freedom etc. Furthermore, it also suggests the realization of a spherical cavity Optical Parametric Oscillator (OPO) emitting a non-thermal,  $E$ -ring distribution

of entangled photon states. Some of these ideas are presently being investigated in our Laboratory.

### III. GENERATION AND TOMOGRAPHIC CHARACTERIZATION OF WERNER STATES

Because of the peculiar spatial superposition property of the output state shown by the structure of Eq. (5), the present apparatus appears to be an ideal source of *any* bi-partite, two-qubit entangled state, either *pure* or *mixed*. In particular of the Werner state [20]:

$$\rho_W = p|\Psi_-\rangle\langle\Psi_-| + \frac{1-p}{4}\mathbf{I}_4 \quad (7)$$

consisting of a mixture of a *pure* singlet state  $|\Psi_-\rangle = 2^{-\frac{1}{2}}\{|HV\rangle - |VH\rangle\}$  with probability  $p$  ( $0 \leq p \leq 1$ ) and of a fully *mixed-state* expressed by the unit operator  $\mathbf{I}_4$  defined in the 4-dimensional Hilbert space. The corresponding density matrix, expressed in the basis  $|HH\rangle, |HV\rangle, |VH\rangle, |VV\rangle$  is:

$$\rho_W = \begin{pmatrix} A & 0 & 0 & 0 \\ 0 & B & C & 0 \\ 0 & C & B & 0 \\ 0 & 0 & 0 & D \end{pmatrix} \quad (8)$$

with:  $A=D=\frac{1}{4}(1-p)$ ,  $B=\frac{1}{4}(1+p)$ ,  $C=-p/2$ . The Werner states possess a highly conceptual and historical value because, in the probability range  $[1/3 < p < 1/\sqrt{2}]$ , they *do not* violate any Bell's inequality in spite of being in this range *nonseparable* entangled states, precisely *NPT states* [17].

How to synthesize by our source these paradigmatic, utterly remarkable states ?

Among many possible alternatives, we selected a convenient *patchwork* technique based again on the quantum superposition principle. This procedure requires only the three optical elements shown in the grey regions of Fig. 1. They were arranged in the experimental layout according to the following steps:

[1] Making reference to the original *source-state* expressed by Eq.(2), a *singlet* state  $|\Psi_{-}\rangle$  was easily obtained by inserting a  $\vec{\pi}$ -flipping, zero-order  $\lambda/2$  wp in front of detector  $B$ .

[2] A anti-reflection coated glass-plate  $G$ ,  $200\mu\text{m}$  thick, inserted in the  $d$  – section with a variable trasverse position  $\Delta x$ , introduced a decohering fixed time-delay  $\Delta t > \tau_{coh}$  that spoiled the *in-principle indistinguishability* of the *intercepted portions* of the overlapping *quantum-interfering* radiation cones, represented by the  $\mathbf{B} + \mathbf{C}$  sectors of the  $E$ -ring in Fig.5. The distinguishability issue is easily solved by thinking that the induced  $\Delta t$ –delay allows, *in principle* an *ideal* detector, i.e. with infinite time resolution, to identify the  $\mathbf{k}$ -cone from which the detected particle came from.

As a consequenced in the intercepted sector  $\mathbf{B} + \mathbf{C}$ , the statistical mixture  $\frac{1}{2} [|H_1, V_2\rangle \langle H_1, V_2| + |V_1, H_2\rangle \langle V_1, H_2|]$  was generated, while the non intercepted sector  $\mathbf{A}$  expresses the polarization *pure-state* singlet contribution to  $\rho_W$ . In other words, *all non-diagonal* elements of  $\rho_W$  contributed by the surface sectors  $\mathbf{B} + \mathbf{C}$  of the E-ring, the ones optically intercepted by  $G$ , were set to *zero* while the non intercepted sector  $\mathbf{A}$  expressed the *pure-state* singlet contribution to  $\rho_W$ .

[3] A  $\lambda/2$  wp was inserted in the semi-cylindrical photon distribution reflected by the beam-splitting prism towards the detector  $A$ . Its position was carefully adjusted in order to intercept *half* of the  $\mathbf{B} + \mathbf{C}$  sector, i.e. by making  $\mathbf{B} = \mathbf{C}$ . Note that only *half* of the E-ring needed to be intercepted by the optical plates, in virtue of the EPR nonlocality. In summary, the sector  $\mathbf{A}$  of the  $E$ -ring contributes to  $\rho_W$  with a *pure* state  $p|\Psi_{-}\rangle \langle \Psi_{-}|$ , the sector  $\mathbf{B} + \mathbf{C} = 2\mathbf{B}$  with the statistical mixture:  $\frac{1-p}{4} \{ [|H_1, V_2\rangle \langle H_1, V_2| + |V_1, H_2\rangle \langle V_1, H_2|] + [|H_1, H_2\rangle \langle H_1, H_2| + |V_1, V_2\rangle \langle V_1, V_2|] \}$  and the probability  $p$ , a monotonic function of  $\Delta x$  ( $p \propto \Delta x$  for small  $p$ ), could be easily varied over its full range of values, from  $p = 0$  ( $\rho_W = \frac{1}{4}\mathbf{I}_4$ ) to  $p = 1$  ( $\rho_W = |\Psi_{-}\rangle \langle \Psi_{-}|$ ) [29]. Optionally, the setting of the  $\lambda/2$  wp intercepting the beam towards  $A$  could be automatically activated by the *single* setting  $\Delta x$ , e.g. via an electromechanical servo.As an example, we may give a detailed demonstration of the feasibility of our technique by synthesizing the identity matrix

**I** (Fig. 6). First insert the  $\lambda/2$  wp on channel  $A$  to intercept  $\frac{1}{4}$  of the  $E$ -ring: in this way the mixture  $\frac{1}{2} [|\Phi_{-}\rangle\langle\Phi_{-}| + |\Psi_{-}\rangle\langle\Psi_{-}|]$  is produced (Fig 6a). The complete erasure of *non diagonal* elements of the matrix is then performed by making a  $\Delta t$ -delay glass plate  $G$  to intercept half of the  $E$ -ring (Fig. 6b)

Any Werner state could be realized by a similar *patchwork* technique, by setting  $\mathbf{B} = \mathbf{C}$  and by adjusting the value of  $p(\Delta x)$ . Far more generally, *all possible* bi-partite states in  $2 \times 2$  dimensions could be created by this technique, as we shall see shortly. This indeed expresses the "universality" of our source.

The tomographic reconstructions [21] of three different Werner states are shown in Fig. 7, with weight  $p = 0.82$  (a),  $p = 0.47$  (b) and  $p = 0.27$  (c). The imaginary components are negligible.

As anticipated at the beginning of the present Section, the Werner states have been introduced as examples of non separable states that, in a proper range of  $p$ , do not violate CHSH inequality. These states are also important for quantum information, since they model a decoherence process occurring on a singlet state travelling along a noisy channel [22].

We may investigate these processes with some details on the basis of some relevant entropic properties of the mixed states. A relevant property of any mixed-state, the "tangle"  $T = [C(\rho)]^2$ , i.e. the square of the *concurrence*  $C(\rho)$ , is directly related to the *entanglement of formation*  $E_F(\rho)$  and expresses the degree of entanglement of  $\rho$  [30]. Another important property of the mixed-states is the "linear entropy"  $S_L = d(1 - Tr\rho^2)/(d - 1)$ ,  $S_L = (1 - p^2)$  for the Werner states, which quantifies the degree of disorder, viz. the *mixedness* of a system with dimensions  $d$  [31]. In virtue of the very definition of  $C(\rho)$ , these two quantities are found to be related, for the Werner states, as follows:

$$T_W(S_L) = \begin{cases} \frac{1}{4}(1 - 3\sqrt{1 - S_L})^2 & \text{for } 0 \leq S_L \leq \frac{8}{9}, \\ 0 & \text{for } \frac{8}{9} \leq S_L \leq 1. \end{cases} \quad (9)$$

Since  $T = 0$  iff the state is separable, we deduce that the Werner states are not separable in the range  $0 \leq S_L < \frac{8}{9}$  or, equivalently, in the range  $\frac{1}{3} < p \leq 1$ . Several Werner states have been generated by this technique and relative experimental values are plotted in the  $T$  vs.  $S_L$  plane shown in Fig. 8 [32]. The agreement between experimental data and theoretical curve appears to be good.

We have recently adopted Werner states generated by this technique to perform the first experimental realization of the "entanglement witness", a powerful method to detect entanglement with few local measurements [33].

#### IV. GENERATION AND TOMOGRAPHIC CHARACTERIZATION OF MEMS

As a final demonstration of the universality of our method, a full set of Maximally entangled Mixed States (MEMS) has been synthesized by our source and tested again by quantum tomography [21,23,34]. On the other hand, according to the introductory notes expressed above, the MEMS are to be considered, for practical reasons, as peculiar ingredients of modern quantum information because their entanglement can not be increased by any unitary transformation. Since the Werner states share this property they can be assumed to belong to the broader class of MEMS.

This last statement can be proved [35] by expressing the density matrix  $\rho_W$  in terms of the *fidelity*  $F$  representing the overlapping between any Werner state and  $|\Psi_-\rangle\langle\Psi_-|$ :

$$\rho_W = \frac{1-F}{3}\mathbf{I}_4 + \frac{4F-1}{3}|\Psi_-\rangle\langle\Psi_-|. \quad (10)$$

Hence the expression for  $T$  is given by:

$$T(\rho_W) = (\max\{0, 2F-1\})^2 \quad (11)$$

The condition for an entangled state implies that  $\frac{1}{2} < F \leq 1$ , and  $T(\rho_W) = (2F-1)^2$ . A nonlocal unitary transformation expressed in terms of the parameter  $a$ , where  $a \in [\frac{1}{2}, 1]$

$$U|\Psi_-\rangle = |\Psi\rangle = \sqrt{a}|H_1, H_2\rangle + \sqrt{1-a}|V_1, V_2\rangle \quad (12)$$



transforms  $\rho_W$  into the mixture:

$$\rho'_W = U\rho_W U^\dagger = \frac{1-F}{3}I_4 + \frac{4F-1}{3}|\Psi\rangle\langle\Psi|. \quad (13)$$

It has been demonstrated that  $\rho'_W$  is still entangled for  $\frac{1}{2} \leq a < \frac{1}{2} \left(1 + \frac{\sqrt{3(4F^2-1)}}{4F-1}\right)$ .  $T(\rho_W)$  is then maximized for  $a = \frac{1}{2}$ . As a consequence, any Werner state belongs to the class of MEMS.

The MEMS generated and tested by our method are the ones that own *maximum tangle* allowed for a given value of linear entropy. The density matrix  $\rho_{MEMS}$  is represented by the matrix given by Eq. (8) with the parameters:  $A \equiv (1 - 2g(p))$ ,  $B \equiv g(p)$ ,  $C \equiv -\frac{1}{2}p$ ,  $D \equiv 0$ . There:  $g(p) = \frac{1}{2}p$  for  $p \geq \frac{2}{3}$  and  $g(p) = \frac{1}{3}$  for  $p < \frac{2}{3}$ . The expression of  $T$ , obtained by a procedure similar to as the one adopted for Werner states, is

$$T_{MEMS}(S_L) = \begin{cases} \frac{1}{4}(1 + \sqrt{1 - \frac{3}{2}S_L})^2, & \text{for } 0 \leq S_L \leq \frac{16}{27} \\ \frac{4}{3} - \frac{3}{2}S_L, & \text{for } \frac{16}{27} \leq S_L \leq \frac{8}{9}. \end{cases} \quad (14)$$

Two different partition techniques of the *E-ring* have been adopted to generate the MEMS, depending on the singlet weight, either  $p < \frac{2}{3}$  or  $p \geq \frac{2}{3}$ . Let's consider three different experimental steps for  $p < \frac{2}{3}$ .

[1] The  $\lambda/2$  wp was inserted in the semi-cylindrical photon distribution reflected by the beam-splitting prism towards the detector  $A$  in order to divide in equal sectors, the two rings corresponding to the left  $\mathbf{k}$ -cone ( $\mathbf{D} = \mathbf{E} + \mathbf{F}$ , Fig. 12a) and to the right  $\mathbf{k}$ -cone ( $\mathbf{G} = \mathbf{H}$ , Fig. 9b). This generated at the output the statistical mixture:  $|V_1, V_2\rangle\langle V_1, V_2|$ ,  $|V_1, H_2\rangle\langle V_1, H_2|$ ,  $|H_1, H_2\rangle\langle H_1, H_2|$ ,  $|H_1, V_2\rangle\langle H_1, V_2|$ .

[2] Sector  $\mathbf{D}$  of the left  $\mathbf{k}$ -cone, corresponding to  $|V_1, V_2\rangle\langle V_1, V_2|$ , was erased by inserting a right-angle opaque screen (Fig. 9a), while sector  $\mathbf{G}$  of the right  $\mathbf{k}$ -cone, corresponding to  $|H_1, H_2\rangle\langle H_1, H_2|$  was kept unaltered (Fig. 9b).

[3] The glass-plate  $G$  was inserted in the *d - section* of the source in order to intercept a portion  $1 - p$  of the sector  $\mathbf{E}$  of the left  $\mathbf{k}$ -cone,  $\mathbf{F}$  in Fig. 9a. As for the generation of the Werner states, this procedure spoiled the indistinguishability of the intercepted portions of

the overlapping radiation cones. The three identical non-zero diagonal terms, corresponding to sector **G**, and to the sectors overlapped with **H**, **E** and **F** were:  $|H_1H_2\rangle\langle H_1H_2|$ ,  $|V_1H_2\rangle\langle V_1H_2|$ ,  $|H_1V_2\rangle\langle H_1V_2|$ , for  $p$  varying in the range  $0 \leq p < \frac{2}{3}$  by transverse displacement of  $G$ . In this way the ratio between the *E-ring* contributions **E** and **F** in the left **k**-cone could be continuously tuned. The larger the **F** contribution, the larger was the decoherence of the MEMS.

In the case  $p \geq \frac{2}{3}$ , no retarding glass plate was needed to realize the MEMS. By fine adjustment of the  $\lambda/2$  wp the weight  $p$  of the *singlet* could be tuned in the range  $\frac{2}{3} \leq p < 1$  and, for each value of  $p$  the vertical position of the screen needed to be adjusted in order to erase the contribution  $|V_1, V_2\rangle\langle V_1, V_2|$  of sector **D** in Fig. 9c.

An accurate experimental production of the MEMS was found particularly severe likely because of the critical requirements needed for operating on the very boundary between the *allowed* and the *forbidden* region of the  $(S_L, T)$  plane [32]. In this sense any lack of correlation within the singlet contribution limited the quality of MEMS. In our source the BBO crystal axis was oriented in a vertical plane and a strong decoherence effect could arise from spatial walkoff occurring in the NL crystal between the vertically polarized twin photons belonging to the left **k**-cone. This one was associated with the extraordinary index of refraction  $n_e(\zeta)$  of the NL crystal, where  $\zeta$  is the angle between the **k** wv of each photon and the axis direction. This effect, which is also present in the  $\lambda/4$  wp, may be reduced by working with a small aperture angle  $\alpha$  of the emission cone. By varying the BBO axis orientation, in the experiment the MEMS were produced by reducing the cone aperture to the value  $\alpha \simeq 1.4^\circ$ .

The tomographic results shown in Fig.10 reproduces graphically, and with fair accuracy two  $\rho_{MEMS}$  structures with parameters  $p = 0.77$  (a) and  $p = 0.45$  (b), while Fig. 11 shows the experimental behaviour of several experimental MEMS in the  $(S_L, T)$  plane compared with the theoretical curves of Eqq. (9) and (14). The produced states lie closely to the theoretical curve for MEMS, however the agreement between the experimental results and

the theoretical predictions was found at last less satisfactory than for Werner states.

## V. NON LOCAL PROPERTIES OF MEMS

It is possible to investigate the non local properties of MEMS assuming a general formalism, i.e. by following the quantitative test founded by John Bell to verify the completeness of Quantum Mechanics [3]. For two correlated spin  $\frac{1}{2}$  particles, with spin vectors  $\vec{s}_1$  and  $\vec{s}_2$ , the following inequality holds:

$$-2 \leq S = P(\hat{u}_1; \hat{u}_2) - P(\hat{u}_1; \hat{u}'_2) + P(\hat{u}'_1; \hat{u}_2) + P(\hat{u}'_1; \hat{u}'_2) \leq 2 \quad (15)$$

where  $\hat{u}_1$  and  $\hat{u}_2$  are unitary norm vectors related to the angular coordinates  $(\Theta_1, \Phi_1)$  and  $(\Theta_2, \Phi_2)$  in the Bloch sphere and  $P(\hat{u}_1; \hat{u}_2)$  is the correlation function

$$P(\hat{u}_1; \hat{u}_2) = \langle (\hat{u}_1 \cdot \vec{s}_1)(\hat{u}_2 \cdot \vec{s}_2) \rangle. \quad (16)$$

Note that the angle  $\Theta$  on the Bloch sphere corresponds to the polarization angle  $\theta = \Theta/2$ .

In a density matrix formalism this last one can be written as:

$$P(\hat{u}_1; \hat{u}_2) = \text{Tr}(\rho O_{12}) \quad (17)$$

where  $O_{12} = O_1 \otimes O_2, O_k = \begin{pmatrix} \cos \Theta_k & e^{-i\Phi_k} \sin \Theta_k \\ e^{i\Phi_k} \sin \Theta_k & -\cos \Theta_k \end{pmatrix}, k = 1, 2$ . By choosing  $\Theta_1 = 0, \Theta_2 = \pi/4, \Theta'_1 = \pi/2, \Theta'_2 = 3\pi/4$ , and  $\Phi_1 = \Phi_2 = \Phi'_1 = \Phi'_2 = 0$  this leads to the well known result:  $S = 2\sqrt{2} > 2$  for a spin singlet  $|\Psi_-\rangle$ . In the case of MEMS the very general form of density matrix  $\rho$  given by Eq. (8) can be adopted. There  $A, B, C = -\frac{1}{2}p, D$  are real numbers and  $D$  depends on the normalization condition,  $\text{Tr} \rho = 1: D = 1 - A - 2B$ . The correlation function becomes

$$P(\hat{u}_1; \hat{u}_2) = (1 - 4B) \cos \Theta_1 \cos \Theta_2 - p \cos(\Phi_1 - \Phi_2) \sin \Theta_1 \sin \Theta_2, \quad (18)$$

where the first term depends on the structure of the state by the diagonal term  $B$  while the second term is function of the only singlet weight  $p$  in the mixture. This leads to the following general expression of the Bell parameter:

$$\begin{aligned}
S &= (1 - 4B)[\cos \Theta_1 \cos \Theta_2 - \cos \Theta_1 \cos \Theta'_2 + \cos \Theta'_1 \cos \Theta_2 + \cos \Theta'_1 \cos \Theta'_2] - \\
& p[\cos(\Phi_1 - \Phi_2) \sin \Theta_1 \sin \Theta_2 - \cos(\Phi_1 - \Phi'_2) \sin \Theta_1 \sin \Theta'_2 + \\
& \cos(\Phi'_1 - \Phi_2) \sin \Theta'_1 \sin \Theta_2 + \cos(\Phi'_1 - \Phi'_2) \sin \Theta'_1 \sin \Theta'_2].
\end{aligned} \tag{19}$$

The inequality violation conditions are found by looking for an extremal point of  $S$ . It can be verified that  $\frac{\partial S}{\partial \Theta_k} = 0$  for:  $\cos \Theta_1 = \cos \Theta_2 = \cos \Theta'_1 = \cos \Theta'_2 = 0$ . Set  $\Theta_1 = \Theta'_2 = -\pi/2$ ,  $\Theta'_1 = \Theta_2 = \pi/2$  as a convenient choice and, by substitution, the following expression:

$$S = p [\cos(\Phi_1 - \Phi_2) - \cos(\Phi'_1 - \Phi_2) + \cos(\Phi_1 - \Phi'_2) + \cos(\Phi'_1 - \Phi'_2)]$$

attains its minimum value  $S = -2\sqrt{2}p$  when  $\Phi_1 = -\Phi'_1 = \pi/4$ ,  $\Phi_2 = \pi/2$ ,  $\Phi'_2 = 0$ . Hence we find that the violation of the Bell inequalities is observed only for states with  $p > 1/\sqrt{2}$ , for any values of the diagonal terms  $A, B, D$ .

This result holds for Werner states, where  $A = D = \frac{1}{4}(1 - p)$ ,  $B = \frac{1}{4}(1 + p)$ , as said in Section III.

By a more elegant procedure, we could note that for any traceless operator  $O_{12}$  the expectation value in a state with weight  $p$  is given by

$$P(\hat{u}_1; \hat{u}_2) = \text{Tr}(\rho_W O_{12}) = pP_s(\hat{u}_1; \hat{u}_2). \tag{20}$$

The expression of the Bell inequality then becomes

$$-\frac{2}{p} \leq P_s(\hat{u}_1; \hat{u}_2) - P_s(\hat{u}_1; \hat{u}'_2) + P_s(\hat{u}'_1; \hat{u}_2) + P_s(\hat{u}'_1; \hat{u}'_2) \leq \frac{2}{p}, \tag{21}$$

which is violated for  $p > 1/\sqrt{2}$ , i.e.  $S_L < 1/2$ . The corresponding experimental test requires the same angular setting of the  $\pi$ -analyzer as any standard Bell test performed for a pure singlet state and reported in Section IIB.

Note that a in the range  $p \in [\frac{1}{\sqrt{2}}, \frac{1}{3}]$ , or equivalently in  $S_L \in [\frac{1}{2}, \frac{8}{9}]$ , the Werner states, although not separable, do not violate the CHSH inequality [36].

In summary, for any Werner state,  $\rho_W$  three regions can be distinguished:

$$\frac{1}{\sqrt{2}} < p \leq 1 \quad (0 \leq S_L < \frac{1}{2}) \quad \rho_W \text{ is not separable and violates local realism;}$$

$\frac{1}{3} < p \leq \frac{1}{\sqrt{2}}$  ( $\frac{1}{2} \leq S_L < \frac{8}{9}$ )  $\rho_W$  is not separable and does not violate the CHSH inequality;

$0 \leq p \leq \frac{1}{3}$  ( $\frac{8}{9} \leq S_L \leq 1$ )  $\rho_W$  is separable and local .

The following corresponding values of the  $|S|$  parameter have been obtained experimentally :  $|S| = 2.0790 \pm 0.0042$  (Fig. 7a),  $|S| = 1.049 \pm 0.011$  (Fig. 7b),  $|S| = 0.4895 \pm 0.0047$  (Fig. 7c).

The test of Bell-CHSH inequalities has been performed for several generated Werner states. The relative behaviour of  $|S|$  as a function of the weight  $p$  is shown in Fig. 12. The experimental data, placed under the expected straight line show the effect of a non perfect correlation within the singlet region **A** in Fig.5.

We may extend the above consideration to any MEMS state,  $\rho_{MEMS}$ , where  $A = 1 - 2g(p)$ ,  $B = g(p)$ ,  $D = 0$ . The correlation function becomes

$$P(\hat{u}_1; \hat{u}_2) = (1 - 4g(p)) \cos \Theta_1 \cos \Theta_2 - p \cos(\Phi_1 - \Phi_2) \sin \Theta_1 \sin \Theta_2. \quad (22)$$

In this case the violation,  $p = \frac{1}{\sqrt{2}}$ , occurs for the point with coordinates  $(S_L, T) = (0.552, 0.5)$ . An experimental test of Bell's inequality, performed with these states, involves observables with a complex phase term  $\Phi$ .

Two distinct regions can be distinguished in the case of MEMS:

$\frac{1}{\sqrt{2}} < p \leq 1$  ( $0 \leq S_L < 0.552$ )  $\rho_{MEMS}$  is not separable and violate local realism;  
 $\frac{1}{\sqrt{2}} < p \leq 0$  ( $0.552 \leq S_L < \frac{8}{9}$ )  $\rho_{MEMS}$  is not separable and do not violate CHSH inequality.

## VI. CONCLUSION AND ACKNOWLEDGMENTS

The novel structural characteristics of the SPDC source of  $\pi$ -entangled photon pairs and the new way the quantum superposition principle underlying its performance is exploited, are expected to suggest in the future an increasing number of sophisticated applications in the domain of quantum information, quantum communication and in the broader field

dealing with of the fundamental tests of quantum mechanics. We can think, for instance to the entanglement multiplexing in quantum cryptographic networks, new schemes of joint entanglement over  $\vec{\pi}$  and  $\mathbf{k}$ -vector degrees of freedom etc. As already mentioned, adding a spherical cavity to the new device will allow the realization of a new kind of Optical Parametric Oscillator (OPO) synchronously pumped by a high peak-power, mode-locked femtosecond UV source. This device would generate a multiphoton non-thermal entangled state over a spatially extended *E-ring* distribution of  $\mathbf{k}$ -vectors. As said, this idea is presently being investigated in our Quantum Optics Laboratory in Roma.

We already emphasized that, as far as applications to quantum-mechanical foundations are concerned, the present device appears to be an ideal source of bi-partite *mixed-states*, as reported at length in the present paper, and of bi-partite *non-maximally entangled* states. In this last respect, a comprehensive study on the verification of the *Hardy's ladder proof*, a relevant quantum nonlocality test, has been successfully completed recently [11] and will be reported extensively elsewhere. There the performance of the source was so good as to allow the attainment of the ladder's rung  $K = 20$ , while previous experiments were limited to  $K \leq 3$  [14,37].

In summary, we do believe that the present work may represent a real breakthrough in an important branch of modern science and certainly will lead soon to relevant applications of advanced technology.

Thanks are due to W.Von Klitzing and G. Giorgi for early involvement in the experiment and for useful discussions. This work was supported by the FET European Network on Quantum Information and Communication (Contract IST-2000-29681: ATESIT) and by PRA-INFN 2002 (CLON).

## REFERENCES

- [1] E. Schroedinger, *Proc. Cambridge Phil. Soc.* **31**, 555 (1935).
- [2] L. Rosenfeld, Commentary to EPR (1967) in: *Quantum Theory and Measurement*, J.A. Wheeler and W.H. Zurek eds., (Princeton U. Press, 1983).
- [3] J. S. Bell, *Speakable and Unsayable in Quantum Mechanics* (Cambridge University Press, 1988); A. Aspect, P. Grangier and G. Roger, *Phys. Rev. Lett.* **49**, 91 (1982); M. Jammer, *The Philosophy of Quantum Mechanics* (Wiley, New York, 1974).
- [4] A. Ekert, R. Jozsa, R., *Rev. Mod. Phys.* **68**, 733 (1996); E. Knill, R. Laflamme, G.J. Milburn, *Nature* **409**, 46 (2001).
- [5] C. H. Bennett, G. Brassard, C. Crepeau, R. Jozsa, A. Peres and W. K. Wootters, *Phys. Rev. Lett.* **70**, 1895 (1993).
- [6] D. Boschi, S. Branca, F. De Martini, L. Hardy and S. Popescu, *Phys. Rev. Lett.* **80**, 1121 (1998); D. Bouwmeester *et al*, *Nature (London)* **390**, 575 (1997); I. Marcikic *et al*. *Nature* **421**, 509 (2003).
- [7] A. Ekert, *Nature* **358**, 14 (1992); N. Gisin *et al*. *Rev. Mod. Phys.* **74**, 145 (2002).
- [8] E. Lombardi, F. Sciarrino, S. Popescu and F. De Martini, *Phys. Rev. Lett.* **88**, 070402 (2002); S. Giacomini, F. Sciarrino, E. Lombardi and F. De Martini, *Phys. Rev. A* **66**, 030302 (2002).
- [9] D. Klyshko, *Photons and Nonlinear Optics* (Gordon and Breach, New York, 1988); P. G. Kwiat *et al*. *Phys. Rev. Lett.* **75**, 4337 (1995).
- [10] P. G. Kwiat, E. Waks, A. G. White, I. Appelbaum and P. H. Eberhard, *Phys. Rev. A*, **60**, R773 (1999).
- [11] G. Giorgi, G. Di Nepi, P. Mataloni and F. De Martini, *Laser Physics*, **13**, 350 (2003); M. Barbieri, F. De Martini, G. Di Nepi, P. Mataloni, *e-print quant-ph/0303018*

- [12] E. S. Fry, T. Walther and S. Li, *Phys. Rev. A*, **52**, 4381 (1995).
- [13] D.Bohm, *Quantum Mechanics*, Ch. 23 (Dover, NY 1989).
- [14] L. Hardy, *Phys. Rev. Lett.* **71**, 1665 (1993); D. Boschi, S. Branca, F. De Martini and L. Hardy, *Phys. Rev. Lett.* **79**, 2755 (1997) and: *Phys. Rev.A*, **56**, 176 (1997) and: "Erkenntnis", **45**, 367 (1997).
- [15] C. H. Bennett and S. J. Wiesner, *Phys. Rev. Lett.* **69**, 2881 (1992).
- [16] K.Kraus, *States, Effects and Operations: Fundamental Notions of Quantum Theory* (Wiley, NY 1991).
- [17] A. Peres, *Phys. Rev. Lett.* **77**, 1413 (1996); L. Duan, G. Giedke, J.I. Cirac, P. Zoller, *Phys.Rev.Lett.* **84**,2722 (2000); R. Simon, *Phys. Rev.Lett.* **84**, 2726 (2000).
- [18] M. Lewenstein, D. Bruss, J.I. Cirac, B. Kraus, M. Kus, J. Samsonowicz, A. Sampera and R. Tarrach, *Journal of Mod. Optics*, **47**, 2841 (2000); D. Bruss, J.I. Cirac, P. Horodecki, F. Hulpke, B. Kraus and M. Lewenstein, *Journal of Mod. Optics*, **49**, 1399 (2002)
- [19] M. Horodecki, P. Horodecki and R. Horodecki, *Phys. Rev. Lett.* **80**, 5239 (1998); M. Horodecki, P. Horodecki and R. Horodecki, in: *Quantum Information: An Introduction to Basic Theoretical Concepts and Experiments* (Springer, Berlin 2001).
- [20] R. F. Werner, *Phys. Rev. A* **40**, 4277 (1989)
- [21] D. F. V. James, P. G. Kwiat, W. J. Munro and A. G. White, *Phys. Rev. A*, **64**, 052312 (2001).
- [22] M. A. Nielsen, I. L. Chuang, *Quantum Computation and Quantum Information*, Cambridge (University Press, Cambridge 2000).
- [23] S. Ishizaka, T. Hiroshima, *Phys. Rev. A*, **62**, 022310 (2000); W. J. Munro, D. F. V. James, A.G. White and P. G. Kwiat, *ibid.* **64**, 030302 (2001), F. Verstraete, K. Audenaert and B. De Moor, *ibid.* **64**, 012316 (2001).



- [24] F. De Martini, *Phys.Rev.Lett.***81**, 2842 (1998).
- [25] Y. H. Shih and C. O. Alley, *Phys. Rev. Lett.* **61**, 2921 (1988); Z. Y. Ou and L. Mandel, *ibid.* **61**, 50 (1988).
- [26] J. F. Clauser, M. A. Horne, A. Shimony and R. A. Holt, *Phys. Rev. Lett.*, **23**, 880 (1969).
- [27] E. Santos, *Phys. Rev. Lett.*, **66**,1388 (1991);N. D. Mermin, in *New Techniques and Ideas in Quantum Measurement* (The N.Y.Academy of Sciences, New York, 1986); A. Garuccio, *Phys.Rev.A*, **52**, 2535 (1995).
- [28] C. K. Hong, S. Y. Ou, L. Mandel, *Phys. Rev. Lett.* **59**, 2044 (1987).
- [29] For an alternative realization of Werner state cfr.Y.S.Zhang, Y.F.Huang, C.F.Li and G.C. Guo, *Phys.Rev. A* **66**, 062315 (2002).
- [30] W. K. Wootters, *Phys. Rev. Lett.* 80, 2245, (1998); S. Bose and V. Vedral, *Phys. Rev. A.* **61**, 040101(2000); V. Coffman, J. Kundu, W. K. Wootters, *ibid.* **61**, 052306 (2000). Since  $E_F(\rho)$ ,  $C(\rho)$ ,  $T$  are monotonic functions of one another, they are equivalent measures of entanglement.
- [31] T.C. Wei, K. Nemoto, P. M. Goldbart, P. G. Kwiat, W. J. Munro, F. Vestraete, *Phys. Rev. A* **67**, 022110 (2003).
- [32] A.G. White, D. F. V. James, W. J. Munro and P. G. Kwiat, *Phys. Rev. A.* **65**, 012301(2001).
- [33] M.Barbieri, F.De Martini, G.Di Nepi, P.Mataloni, M.D'Ariano and C.Macchiavello, *quant-ph/0307003*, subm. to *Phys.Rev.Lett*; O. Gühne, P. Hyllus, D. Bruß, A.Ekert, M. Lewenstein, C.Macchiavello, and A. Sanpera, *Phys. Rev. A* **66**, 062305 (2002).
- [34] P. Kwiat, J. Altepeter, D. Branning, E. Jeffrey, N. Peters, T. C. Wey, *quant-ph/0303040*.
- [35] T. Hiroshima, S. Ishizaka, *Phys. Rev. A*, **62**, 044302 (2000).

[36] J. Barrett, *Phys. Rev. A*, **64**, 042305 (2001).

[37] A. G. White, D. F. V. James, P.H. Eberhard and P. G. Kwiat, *Phys. Rev. Lett.*, **83**, 3103 (1999).

## VII. APPENDIX A

**Phase Control of the Entangled state.** Because of its peculiar configuration of single arm interferometer the high brilliance source overcomes many of the instability problems due to the typical phase fluctuations of a standard two arm interferometer. The spherical mirror  $M$  determines a large value of the displacement,  $|\Delta d| \simeq 60\mu m$  in our case, which allows the phase transition  $\phi = 0 \rightarrow \phi = \pi$  from Bell state  $|\Phi_+\rangle$  to the other  $|\Phi_-\rangle$ . This can be demonstrated by referring to Fig. 13. Starting from the condition  $d = R$  and neglecting for simplicity the BBO and  $\lambda/4$  wp thickness, a displacement  $\Delta d = OO' = AA' \neq 0$  determines different optical paths of the UV beam,  $2(OA')$ , and of the photon pair generated toward the left in Fig.13 and reflected by mirror  $M$ ,  $2(OB' + B'C)$ . The factor 2 which compares in the second optical path accounts for the two photon emission over two symmetric directions with respect  $\mathbf{k}_p$ . Phase difference has the following expression:

$$\phi = 4\pi(OA')\lambda_p^{-1} - 4\pi(OB' + B'C)\lambda^{-1} = 4\pi\lambda^{-1} [2(OA') - (OB' + B'C)].$$

$\phi$  is function of the distances  $OA'$ ,  $OB'$  and  $B'C$ . Since  $OA = OB = OA' = OB' = R$ , we have:  $OA' = R + \Delta d$ . By approximating  $\alpha'' \cong \alpha' \cong \alpha$  and applying the Carnot theorem to the triangle  $OO'B'$ , we find the following expression:  $OB' = \sqrt{(\Delta d)^2 + R^2 + 2R\Delta d \cos(\alpha)}$  Finally the following equality holds:  $B'C = O''C + O''B'$ , and it can be easily found:  $(O''B') = -(OO'') \cos(\alpha) + (OB')$ , while  $O''C$  is obtained by simple calculations.

By the above results we easily find that the transition  $|\Phi_+\rangle \rightarrow |\Phi_-\rangle$  is obtained by a displacement  $|\Delta d| = 60\mu m$ , which is in good agreement with the experimental results.

Note that the condition  $\Delta d \neq 0$  implies a lateral displacement  $OC$  of the reflected SPDC beams. Because of the intrinsic cylindrical symmetry,  $OC$  may be viewed as the radius of an annular region which grows with  $\Delta d$  on the BBO plane. This geometrical effect makes the two emission cones distinguishable. It introduces a *spatial* decoherence which becomes relevant as far as  $OC$  becomes comparable with the diameter of the *active* pumped region of the crystal ( $\simeq 150\mu m$ ). In our experimental conditions,  $OC \simeq 10^{-1}\Delta d$ , we have observed that any coherent superposition on the state vanishes for  $|\Delta d| \gtrsim 600\mu m$ .

### Figure Captions

**Fig. 1** - Layout of the universal, high-brilliance source of polarization entangled photon states and of general mixed states. Inset: Entanglement-ring and pinhole of radius  $r$  for spatial selection.

**Fig. 2** - Bell inequalities test. The selected state is  $|\Phi_{-}\rangle = \frac{1}{\sqrt{2}}(|H_{1}, H_{2}\rangle - |V_{1}, V_{2}\rangle)$ .

**Fig. 3** - Coincidence rate versus the position  $X$  of the beam splitter in the Ou-Mandel experiment. In the inset the corresponding interferometric apparatus is shown. The selected state is  $|\Psi\rangle = \frac{1}{\sqrt{2}}(|H_{1}, V_{2}\rangle + e^{i\phi}|V_{1}, H_{2}\rangle)$ .

**Fig. 4** - Plot of the fringe visibility (circles, left axis) and coincidence rate (squares, right axis) as a function of the iris diaphragm radius  $r$ .

**Fig. 5** - Partition of the (half)  $E$ -ring for Werner states production.

**Fig. 6** - Tomographic reconstruction (real parts) of the mixtures  $\frac{1}{2}[|\Phi_{-}\rangle\langle\Phi_{-}| + |\Psi_{-}\rangle\langle\Psi_{-}|]$  (a) and  $\frac{1}{4}\mathbf{I}_{4}$  (b).

**Fig. 7** - Tomographic reconstruction (real parts) of three different Werner states. Corresponding singlet weights  $p$  are also shown.

**Fig. 8** - *Tangle* vs *Linear Entropy* for experimentally generated Werner states. Continuous line corresponds to the theoretical curve.

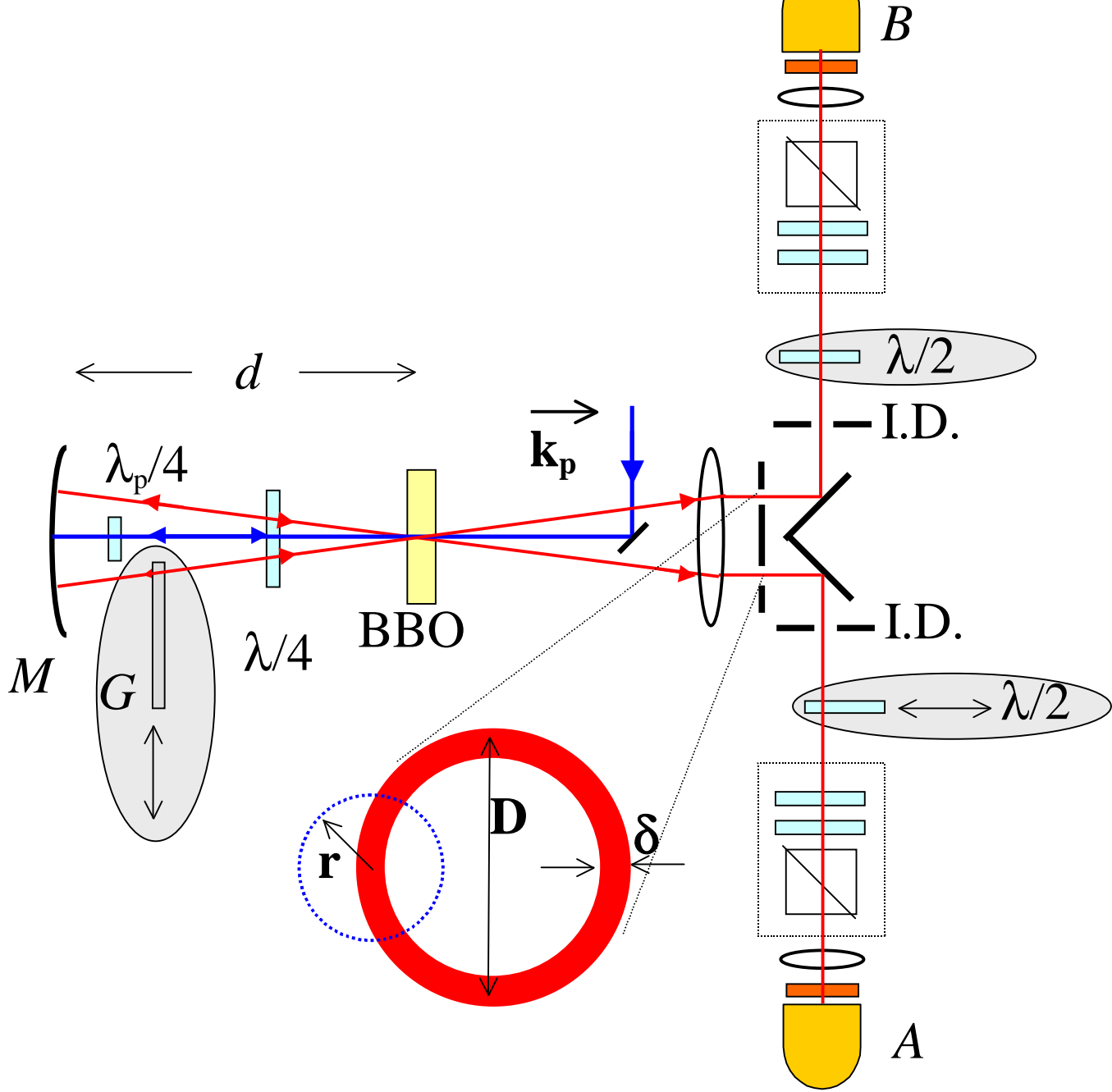
**Fig. 9** - Partition of the (half) *E-ring* for MEMS production: (a) left cone for  $0 \leq p \leq \frac{2}{3}$ , (b) right cone, (c) left cone for  $\frac{2}{3} \leq p \leq 1$ .

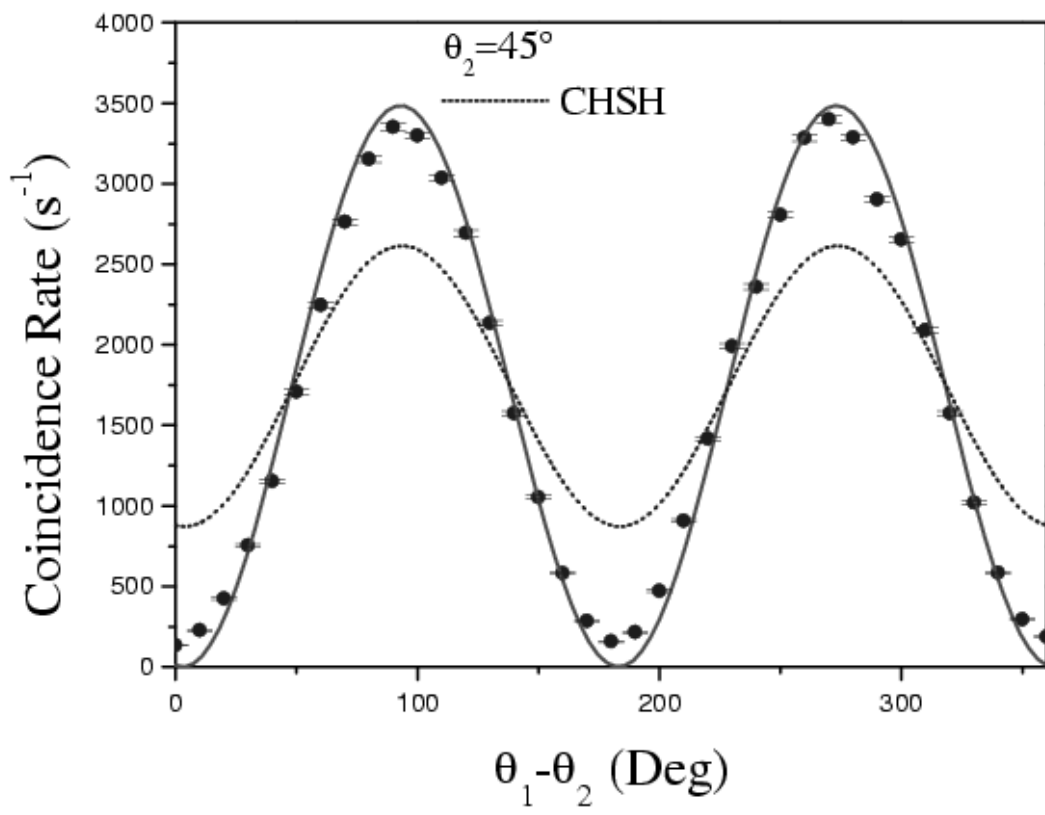
**Fig. 10** - Tomographic reconstruction (real parts) of two different MEMS. Corresponding singlet weights  $p$  are also shown.

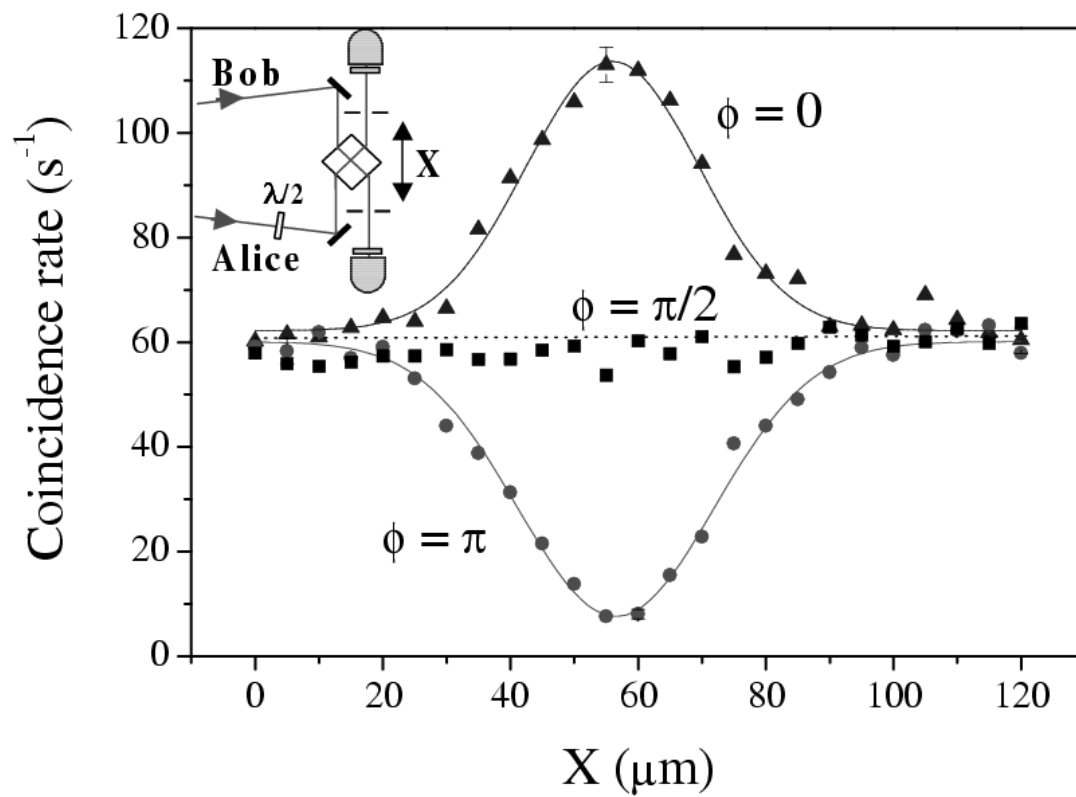
**Fig. 11** - *Tangle vs Linear Entropy* for experimentally generated MEMS. Continuous line represents theoretical behaviour, dotted line is the expected curve for Werner states.

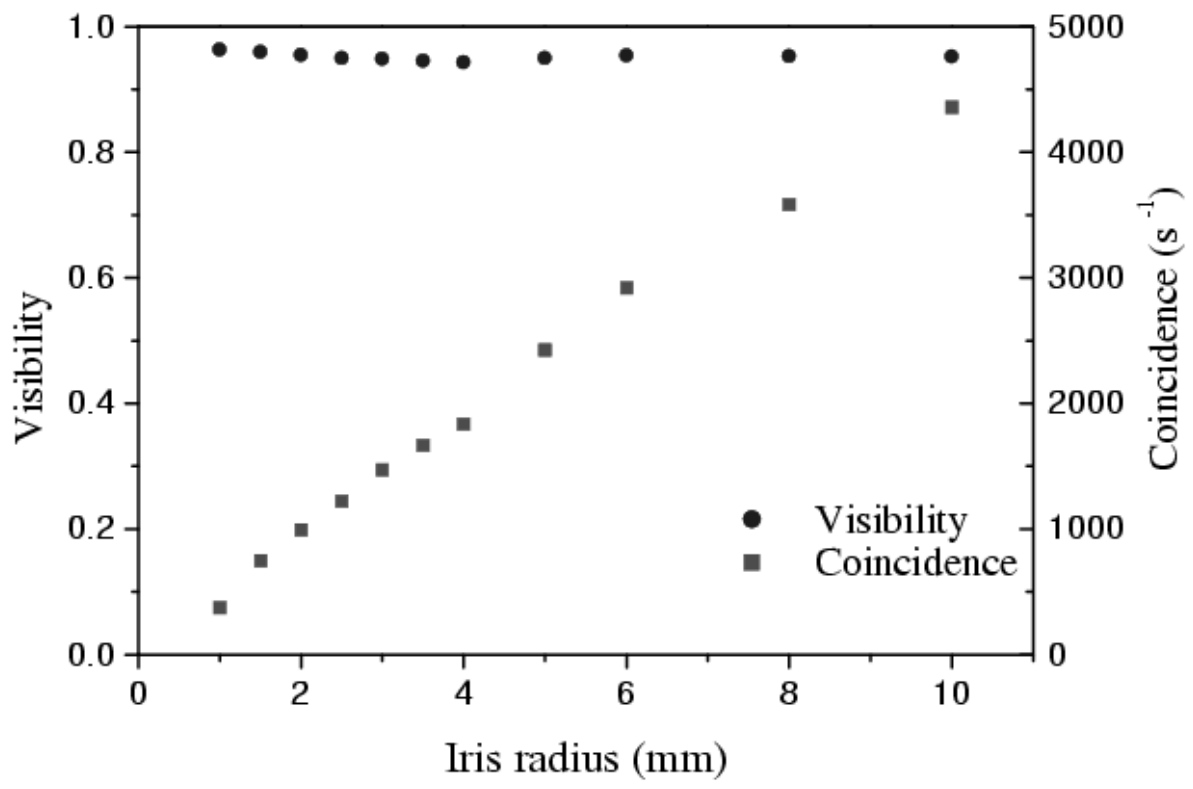
**Fig. 12** - Plot of the Bell parameter  $|S|$  as a function of weight  $p$ . The expected straight line  $|S| = 2\sqrt{2}p$  is also reported.

**Fig. 13** - Scheme representing the optical path difference within the single arm interferometer.

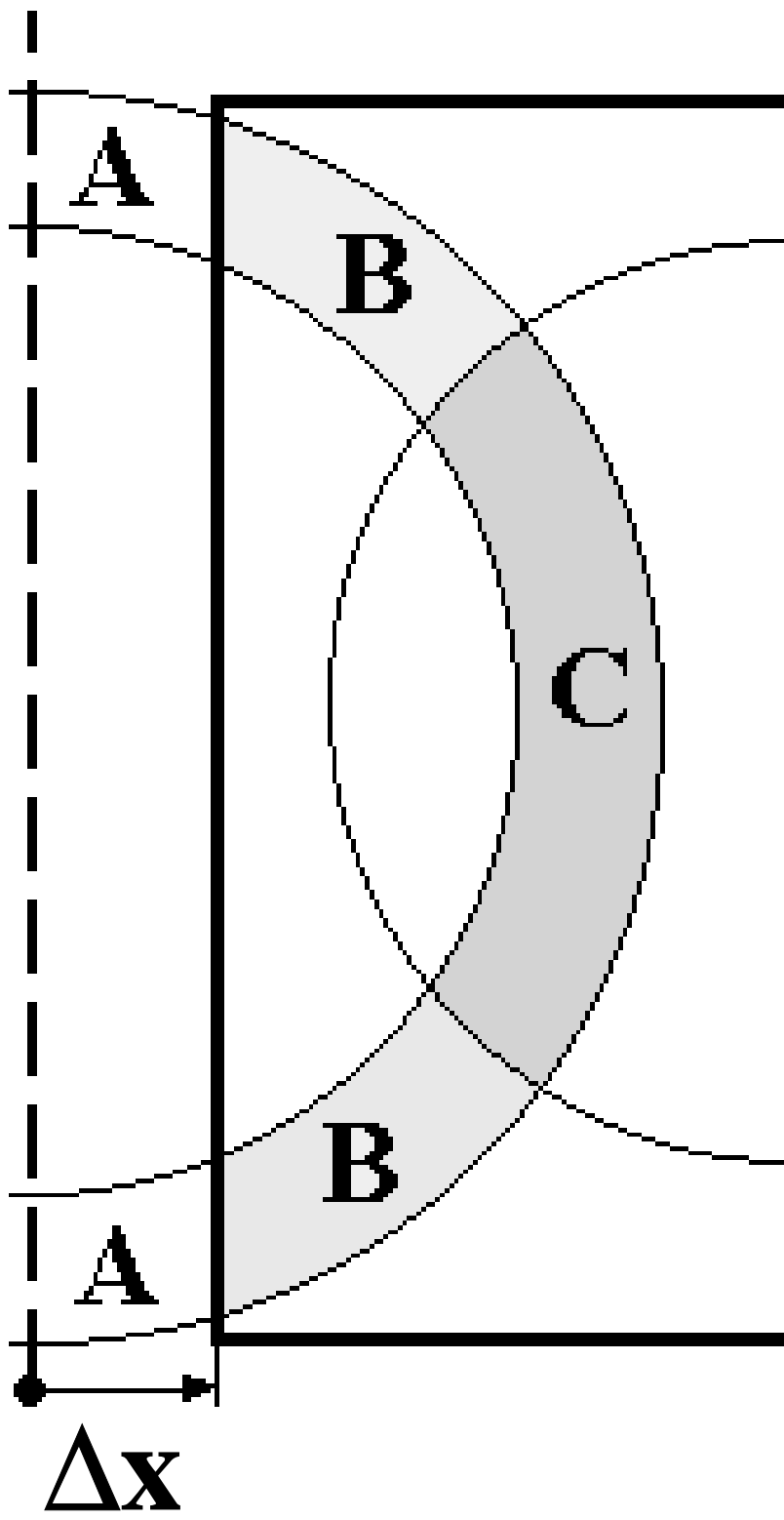


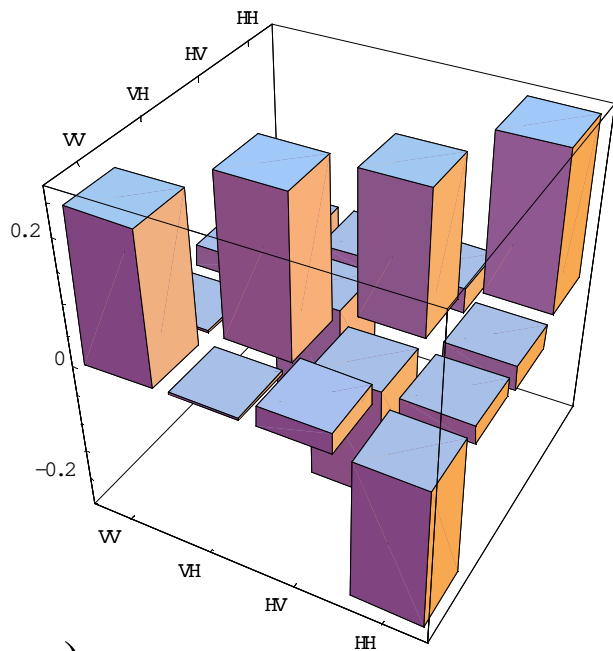




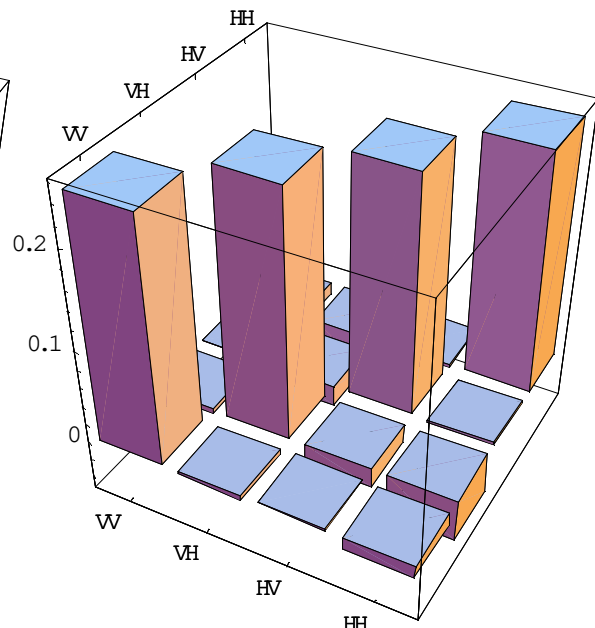




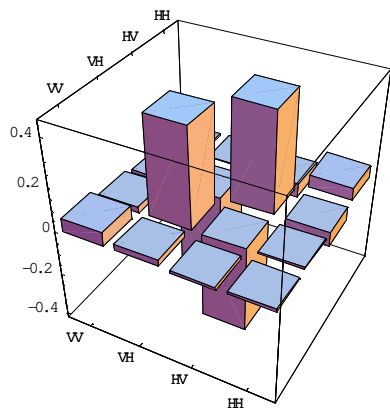




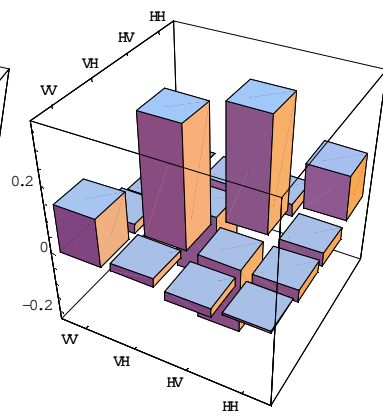
a)



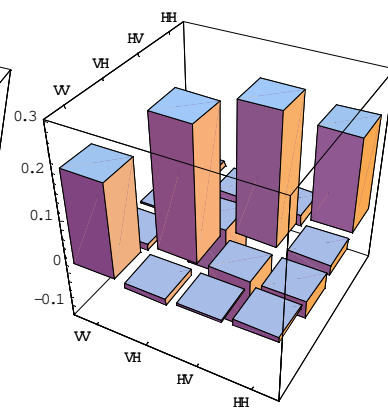
b)



a)  $p=0.82$



b)  $p=0.47$



c)  $p=0.27$

